A Direct Sampling Mass Spectrometer Investigation of Oxidation Mechanisms for Acetic Acid in Supercritical Water

Sean P. Maharrey*,† and David R. Miller

Chemical Engineering Program, Department of Mechanical and Aerospace Engineering, 0411 University of California San Diego, 9500 Gilman Drive, La Jolla, California 92093-0411

Received: December 15, 2000; In Final Form: March 28, 2001

A quartz capillary microreactor is directly coupled to a mass spectrometer utilizing the exit of the reactor as a standard high-pressure free-jet molecular beam source. This direct sampling mass spectrometry (DSMS) design is used to probe the reaction mechanism for the oxidation of acetic acid in supercritical water. The DSMS system is able to probe reactor conditions and to detect reaction intermediates, radicals, and product species during the early stages of reaction at the extreme pressures (>23 MPa) and temperatures (400−500 °C) of interest to supercritical water oxidation. The oxidation of acetic acid with hydrogen peroxide in supercritical water was selected as a prototypical oxidation reaction to validate our DSMS design. We report on our initial results, which include (1) the complete decomposition of the hydrogen peroxide to oxygen before 450 °C, (2) the subsequent onset of reaction at 470 °C, (3) the identification and measurement of the HO_2* radical, indicating hydrogen abstraction by oxygen as the dominate initiation step, and (4) the lack of any bulk water incorporation into the reaction mechanism up to 500 °C.

Introduction

Supercritical water oxidation (SCWO) is a relatively new technology for the destruction of toxic organic wastes. The organic contaminant and oxidizer are both completely miscible with supercritical water and the resulting single-phase reaction environment supports a very efficient oxidation reaction, proceeding to greater than 99% completion, and minimizes the formation of equally harmful byproducts. To scale-up existing bench-scale reactors to full-scale facilities, the oxidation kinetics of a given oxidation reaction must be well understood.[1−4] Aki and Abraham,[5] Cansell et al.,[6] and Rice and Steeper[7] give results for the oxidation kinetics of model industrial compounds in supercritical water.

Current reactor designs used for SCWO are generally based on closed-loop flow reactors. With these designs, the reactor effluent is sampled only after being quenched by a heat exchange, to reduce temperature, followed by expansion through a throttling valve, to reduce pressure. This results in a flow separation and the subsequent recovery of a two-phase effluent stream. The recovered liquid phase is generally sampled and analyzed by HPLC, while GC is used for the gas phase. An example of this type of reactor design is that used by Tester[8] and his group at MIT.

The HPLC and GC techniques for analyzing the reactor effluent are limited in that they can only detect remaining reactants and stable product species—unstable and short-lived intermediates and radicals are not observed with these techniques. Also, the temperature and pressure reduction processes have typical residence times on the order of seconds, not necessarily favorable conditions for quenching the oxidation reaction. Second-generation flow reactor designs incorporate optical diagnostics directly into the heated zone of the reactor and have been able to observe a limited number of intermediate species.[9−11]

Most direct optical spectroscopy to date has centered on the use of vibrational spectroscopy using laser excitation to detect species in solution under supercritical conditions. The changes in the spectrum of many different species can be monitored simultaneously with relatively good sensitivity and selectivity. Fourier transform Raman spectroscopy, using near-IR detectors instead of the traditional visible light detectors of conventional Raman, and conventional FTIR both have the wide spectral windows and resolution in time to study the rates of change of many species in solution simultaneously.

The direct optical spectroscopy technique must deal with the corrosiveness of the supercritical water in the design and integrity of the optical windows requiring glass-to-metal seals. The metals used to make the seals deteriorate significantly upon prolonged exposure to the supercritical water environment.[12,13] Especially problematic with direct optical spectroscopy, is the calibration of the "hot" band structures for a given species in the Raman spectra. Despite these problems, direct optical spectroscopy is still being used for studies of oxidation species in supercritical water. Ikushima and Arai[14] present current work on the use of Raman spectroscopy to study the dynamic behavior of nitrate anion in supercritical water (SCW), while Chlistunoff and Johnston[15] give results for the use of UV−vis spectroscopy to study the dissociation constant of bichromate in SCW.

Our approach to the problem of analyzing the reactant/intermediate/product mixture is to apply direct sampling mass spectrometry (DSMS) as a technique to probe the reaction species present in the supercritical water. DSMS is a powerful technique to use when investigating the individual mechanistic steps involved in the overall oxidation reaction. The DSMS technique is one of the few that can monitor several species at once, has very good sensitivity, and allows for the use of isotopic substitution to elucidate individual mechanistic steps. A disad-

* Author to whom correspondence should be directed.
† Current address: Sandia National Laboratories, P.O. Box 969, MS-9052, Livermore, CA 94551-0969. Tel.: (925) 294-3411. Fax: (925) 294-2276. E-mail: spmahar@sandia.gov.

10.1021/jp004512b CCC: $20.00
Published on Web 05/17/2001

vantage of the DSMS technique is that it must operate under high vacuum. Problems associated with the requirement of operation in a vacuum are the design of the reactor/detector interface and the mass flow into the vacuum system that must be handled by the vacuum pumps.

The experimental challenge was to sample a very high-pressure, supercritical water, supersonic free-jet expansion using standard molecular beam techniques. Following the lead of Groeger and Fenn,[16] who used a micro-jet burner as a molecular beam source for investigating combustion products using FTIR spectroscopy, we designed a microscale capillary flow reactor to act as our molecular beam source and coupled this reactor to the DSMS system to analyze the reactive agents and products present in the supercritical reaction mixture. Using a microscale design, the entire reactor could be easily moved from the benchtop and mounted within the vacuum system, eliminating the problem of designing a coupling interface from vacuum to the high pressure of the supercritical water reactor. The sonic nozzle terminating the quartz capillary flow reactor becomes the free-jet molecular beam source. Others have designed systems that use a supersonic jet molecular beam interface to couple a supercritical fluid chromatograph to a mass spectrometer for product identification.[17−22]

We report on the design and analysis of the quartz capillary microreactor as a benchtop reactor and its use to obtain global kinetic rate parameters elsewhere.[23,24] This paper will focus on the coupling of this microreactor to a 3-stage, differentially pumped vacuum system containing the mass spectrometer and the use of this DSMS system in analyzing the supercritical water oxidation of acetic acid. We are able to report the first direct measurement of the oxidation mechanism, including determination of the initiation step and the extent to which the supercritical water participates in the oxidation mechanism, and we are able to measure selected reaction intermediates, including the $HO_2^{\bullet}$ radical. We use acetic acid as a prototypical reactant to demonstrate the feasibility of the reactor design. Acetic acid was initially thought to be a major intermediate in the overall oxidation of larger molecular weight hydrocarbons and was also considered to be a rate-limiting step in the overall oxidation.[25] However, later research is in conflict with this result.[26,27] We also chose hydrogen peroxide instead of oxygen as the oxidizer. This choice in oxidizer was made simply out of experimental convenience. Hydrogen peroxide can be obtained as an aqueous solution as strong as 30 wt %, which allows for easy sample preparation and an accurate determination of the initial oxidizer concentration.

Experimental Design

Although free-jet molecular beams are well-known, we will provide some details of our design because the DSMS of high-pressure systems is in large part an art which is only guided by classical molecular beam design correlations.

Figure 1 shows the overall direct sampling mass spectrometer system used in the current studies. Included in this figure is the microreactor, along with the key components of the DSMS system. The microreactor is essentially a 20 cm long, 0.050 cm (500μm) inside diameter, 0.0750 cm (750 μm) outside diameter quartz capillary tube with the exit end carefully melted down to form a very short converging nozzle with an exit diameter of about 0.002 cm (20μm). These dimensions result in low flowrates and provide reactor residence times that can be varied over the range of ~1 to 8 s for flowrates of 50−70 mL/h and temperatures and pressures ranging from 400 to 500 °C and 23−25 MPa, respectively. The oxidation reaction occurs in the

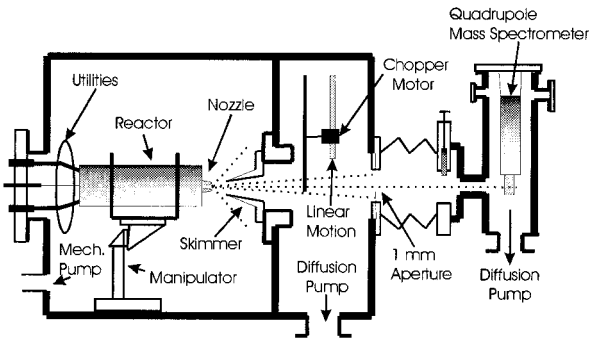

Figure 1. Direct sampling mass spectrometer system.

constant area section of the heated quartz capillary, primarily near the end just before the nozzle, and then it is rapidly quenched in the nozzle and supersonic free-jet expansion.[24] Since the flow times in the nozzle and free-jet expansion scale with the nozzle diameter, these times are small compared with the reactor residence time and result in close to optimal conditions for quenching of the oxidation reaction. Although supercritical water may dissolve quartz in the ppm range we find that these "throw-away" reactors last for at least 20−30 h of operation before any significant change in the reactor flow properties occurs.

The low flowrates also result in low background pressures below 0.030 Torr in the main chamber containing the microreactor during all experimental runs, which helps to minimize problems associated with background gas molecules interacting with the microreactor effluent gases present in the supersonically expanding beam. The small microreactor design is able to achieve supercritical conditions at power levels below 100 W, compared with kwatt levels of more typical reactor designs, which is easily achieved inside the vacuum system or externally on the benchtop. The important experimental inlet variables; pressure, temperature, reactant concentrations, and total mass flowrate, can be very efficiently manipulated with such a small-scale reactor system using standard HPLC components.

The microreactor is mounted within the main chamber of a differentially pumped 3-stage vacuum system and is rigidly supported by an $x-y-z$ manipulator that is used to align the free-jet with the beam line defined by the skimmer, aperture, and mass spectrometer ionizer. This beam line determines the direct line-of-sight for the microreactor effluent beam and the mass spectrometer detector. Utilities, including supercritical fluid delivery and reactor power are brought through the back flange of the main a vacuum chamber. After the free-jet expands into the main a vacuum chamber, a skimmer is used to sample the centerline of the expansion and permit a molecular beam to pass through to the mass spectrometer. The skimmer is 2.01 cm in height, has a 47° interior angle, a 0.036 cm tip opening, and a 0.004 cm wall thickness at the tip.

The skimmed beam passes into the second chamber where it is mechanically chopped by a motor driven wheel. This modulated beam is then collimated by an aperture with a 1 mm diameter hole, located on the back wall of the second "chopping" chamber. The collimated beam then enters the third chamber where it passes through the ionizer of an Extranuclear model quadrupole mass spectrometer.

The main chamber of the vacuum system is pumped by a 170 L/s Roots blower, backed by a 35 ft^3/min (cfm) mechanical pump, with a liquid nitrogen cold trap between the two pumps to capture the water pumped from the main chamber. A 600 L/s 4 in. diffusion pump with water baffle backed by a 15 cfm mechanical pump is used to pump the second chopping chamber.

The mass spectrometer is pumped by a 300 L/s 2 in. diffusion pump with liquid nitrogen baffle backed by a 10 cfm mechanical pump. With this system, water beams with source conditions of 23 MPa and 500 °C were produced that gave background pressures of less than 0.030 Torr in the main chamber, less than 3×10^{-7} Torr in the chopper chamber and less than 5×10^{-8} Torr in the mass spectrometer chamber. The baseline pressures in these chambers were typically under 0.001 Torr, 7×10^{-8} Torr, and 1×10^{-8} Torr, respectively.

For such high-pressure free-jets exiting into high ambient vacuum pressures of less than 0.030 Torr, the distance from the nozzle exit to the skimmer inlet is a critical parameter because of the occurrence of shock waves, especially the normal Mach disk shock along the jet centerline.[28] We found that for optimal beam intensity both the axial and radial nozzle positions had to be set to within 1 mm, which is about 50 nozzle diameters. Typically, the Mach disk in the undisturbed free-jet would occur near 3 cm downstream from the nozzle exit. However, the optimal skimmer location was near 0.5 cm, well within the shock structure of the free-jet expansion.

The skimmer is the most important part of the free-jet sampling process since it provides a buffer between the collision-dominated jet expansion and the collisionless molecular beam that passes through to the mass spectrometer. Although the geometric parameters of the skimmer noted above are all important to a successful design, we found that the wall thickness at the skimmer tip was especially critical on these high-density supercritical expansions. A full discussion of the skimmer design and electropolishing technique used to sharpen the skimmer tip and the resulting improvement in the signal-to-noise are presented elsewhere.[23]

The mass spectrometer experiments involved primarily two types of system configurations. We first conducted molecular beam pulsed time-of-flight (TOF) velocity distribution calibration experiments using initially helium and argon, and later, water. The second set of experiments was standard lock-in amplifier detection using square-wave (SW) modulation for the detection of the oxidation reaction species. Mass spectrometer control and overall experiment control was the same in each type of experiment, only the processing of the electron multiplier detection output was altered. The chopper wheel had both narrow TOF slots and equal on−off slots so that the diagnostic could be readily switched in-situ between the two types of experiments.

TOF is a standard molecular beam technique for determining the velocity distribution of molecules within a molecular beam.[28] We can determine both the mean velocity and translational temperature of our beams with this TOF setup. With these data, we can accurately calculate the beam stagnation temperature, corresponding to the maximum temperature within the microreactor, by the application of a simple energy balance. Helium and argon were both used in a set of TOF experiments to obtain a calibration of the quartz capillary microreactor heating source. For polyatomic gases, like water, internal energy relaxation complicates the TOF analysis considerably and does not permit a unique calculation of the microreactor's stagnation temperature. The results from the TOF experiments will not be presented here and are only mentioned for completeness. A discussion of the TOF experiments and corresponding results can be found elsewhere.[23]

The SW modulation experiment is a standard technique for molecular beam mass spectrometry and for the rapid detection of multiple signals resulting from the different components within a molecular beam. These species component signals can be very small compared to the principle beam species, water in our case. Since the beam is modulated at a known and controlled frequency, a lock-in amplifier, tuned to the proper frequency and phase of the signal, is able to extract data with S/N $< 10^{-3}$. Electronic data processing is discussed elsewhere.[23]

With the DSMS technique, we were able to use isotopic substitution of the acetic acid and water to help probe the oxidation mechanism. Oxidation reactions were conducted with combinations of unlabeled, and isotopically labeled reactants and water and included the following reactant solutions: $H_2O/CH_3COOH/H_2O_2$, $H_2O/CD_3COOD/H_2O_2$, and $D_2O/CH_3COOH/H_2O_2$.

Acetic acid was obtained from Fischer Scientific in glacial form, assayed at greater than 99.5% concentrated, while the hydrogen peroxide, also from Fischer, was received as an assayed solution that was typically in the range of 32−34 wt % in water. Solutions were made by mixing the glacial acetic acid and hydrogen peroxide with ultrapure water to make the required solution concentration of acetic acid and hydrogen peroxide. The ultrapure water was made in-house by distilling deionized water in a Corning Mega-Pure System model MP-3A still. Isotopic compounds, fully deuterated acetic acid (CD_3COOD) and deuterated water, were obtained from Alfa-Aesar with the tagged acetic acid received as glacial, assayed at greater than 99% concentrated and 99.5% fully deuterated, and the tagged water was assayed at 99.5% fully deuterated.

Acetic Acid Oxidation Mechanism

Starting with the lumped mechanism for the SCWO of acetic acid using oxygen as the oxidizer proposed by Boock and Klein,[29,30] we designed an experimental approach to investigate some of the important steps in this mechanism. We first introduced two additional steps into the mechanism to account for the choice of oxidizer, hydrogen peroxide, and to include water as a reactant. We included the decomposition mechanism of hydrogen peroxide given by Lin et al.[31] In Lin's mechanism, hydrogen peroxide undergoes two separate reactions, thermal decomposition to produce oxygen and a free-radical decomposition to produce the $HO^{\bullet}$ radical. The complete mechanism of Boock et al. itself represents a reduced set of rate limiting steps and, with our additions, is a 22 step mechanism for the oxidation of acetic acid. Here we only write down a few of the steps that are most relevant to this study, omitting 13 steps, which includes the H-abstraction, decomposition, and radical recombination. Including the complete oxidation of the methyl radical to CO_2 and H_2O, which also generates CO, the mechanism for the complete oxidation of acetic acid to CO_2 and H_2O requires more than 50 steps.

Hydrogen Peroxide Decomposition:

$$H_2O_2 \rightarrow {}^1/_2O_2 + H_2O \quad (1)$$

$$H_2O_2 \rightarrow 2HO^{\bullet} \quad (2)$$

Initiation:

$$CH_3COOH + O_2 \rightarrow CH_3COO^{\bullet} + HO_2^{\bullet} \quad (3)$$

$$CH_3COOH + HO^{\bullet} \rightarrow CH_3COO^{\bullet} + H_2O \quad (4)$$

Oxygen Addition:

$$CH_3^{\bullet} + O_2 \rightarrow CH_3OO^{\bullet} \quad (5)$$

Isomerization:

$$CH_3OO^{\bullet} \rightarrow C^{\bullet}H_2OOH \quad (6)$$

β-Scission:

$$CH_3COO^{\bullet} \rightarrow CH_3^{\bullet} + CO_2 \quad (7)$$

$$C^{\bullet}H_2OOH \rightarrow H_2C{=}O + HO^{\bullet} \quad (8)$$

Water Gas Shift:

$$CO + H_2O \rightarrow CO_2 + H_2 \quad (9)$$

As indicated above, two additional reactions were added to the mechanism of Boock et al., the decomposition of hydrogen peroxide and the water gas shift reaction. Since Boock was using oxygen as the oxidizer, no initial concentration of the $HO^{\bullet}$ radical was available to contribute to the initiation step involving hydrogen abstraction from the acetic acid hydroxyl group. This reaction, however, was included by Boock under the hydrogen abstraction sequence, which becomes important when enough $HO^{\bullet}$ radical is generated within the early reaction steps. With hydrogen peroxide as the oxidizer, both oxygen and the $HO^{\bullet}$ radical were initially present and could both be included within the initiation step. The second addition was to include the water gas shift reaction, which is one mechanistic step in which the bulk supercritical water can participate as a reactant.

With this modified reaction scheme, we attempted to answer three basic questions: (1) which is the more dominant of the two initiation steps, (2) can the presence of the mechanistically important $HO_2^{\bullet}$ radical be confirmed, (3) and to what extent does the supercritical water participate in the overall reaction scheme. In the next section, the results from the SW modulation experiments that were conducted to investigate these three questions will be presented.

Results and Discussion

I. Mass Spectrum Baseline and Resolution Experiments. Baseline experiments with pure unlabeled water, deuterated water, and a 50/50 mixture of unlabeled and deuterated water were run and the entire mass spectrum was obtained from *m*/*z* 15−70, to account for the complete range of possible oxidation species that might be present in our experiments. For these baseline experiments, the liquid nitrogen baffle on the mass spectrometer chamber was kept filled throughout the experiment to minimize any hydrocarbon peaks due to backstreaming of the Santovac-5 diffusion pump fluid used in the mass spectrometer chamber oil diffusion pump. In these baseline experiments, the mass ranges from *m*/*z* 15−22, where the unlabeled and deuterated water fragments appear, 28−36, where the O_2^+, HO_2^+, and DO_2^+ peaks appear, and 42−50, where the unlabeled CO_2H^+ (*m*/*z* 45) and deuterated CO_2D^+ (*m*/*z* 46) acetic acid fragment peaks occur, were carefully monitored for background noise and hydrocarbon cracking peaks due to the detection chamber diffusion pump oil. These baseline experiments showed that these mass ranges were free from the influence of hydrocarbon peaks from the Santovac-5 diffusion pump fluid. These baseline results allowed us to unambiguously assign peaks detected in these ranges as originating from the reactants or intermediates present in the oxidation mechanism.

The 50/50 mixture of unlabeled and deuterated water was also used in the baseline experiments to see if hydrogen exchange would take place between the unlabeled and deuterated water leading to the detection of scrambled water peaks (HOD^+).

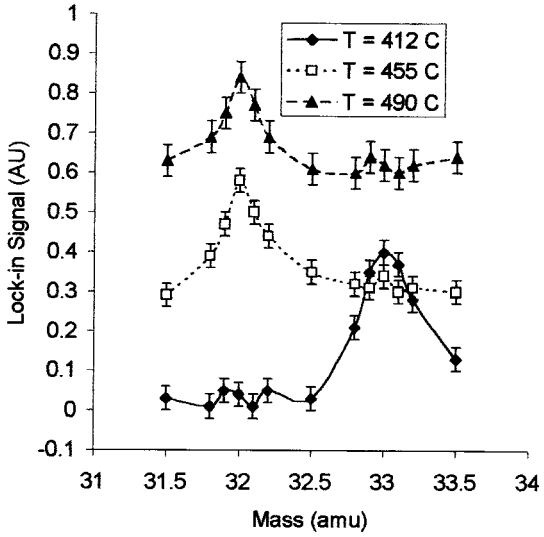

Figure 2. O_2^+ and HO_2^+ sweep signals versus temperature. Experiment conducted with an $H_2O/CH_3COOH/H_2O_2$ sample. Note: the upward baseline shift in the signals as temperature increases is for ease of viewing only.

No water scrambling peaks were detected in any of the baseline experiments, which spanned the entire range of temperature and pressure we used in all the oxidation experiments. Also, during the pyrolysis experiments, discussed below, at least one run in every five was conducted with a 50/50 mixture of unlabeled and fully deuterated acetic acid to monitor the extent of scrambling in the acetic acid that could effect our oxidation measurements. As with the water scrambling tests, no measurable level of scrambling was detected outside the experimental error and was not accounted for in any analysis of the experimental data.

We also examined the mass spectrum for evidence of water clusters formed during the free-jet expansion. Originally we felt such clustering would substantially interfere with the beam-skimmer properties. However, we found no indication of clustering, not even dimer formation, evident in these expansions of supercritical water. Further analysis of the thermodynamics of the free-jet expansion showed that this was to be expected. The adiabatic expansion of the supercritical water does not enter into the two-phase region under our conditions, where clustering is possible, until far downstream in the supersonic expansion where there are too few collisions remaining to generate small clusters.

After these baseline and hydrocarbon cracking pattern calibration experiments were concluded, we switched to discrete mass peak sweep mode experiments using the lock-in amplifier and manual mass mode on the Extranuclear control unit. It was the intent in these experiments to verify that we could achieve adequate resolution of the relevant mass peaks. While most of our data is taken by simply sitting on top of a mass peak, and not by a sweep around each peak, we wish to show one example to verify the mass peak resolution and to indicate the noise level in these experiments. Figure 2 shows the lock-in discrete sweep mode spectrum output for one of the $H_2O/CH_3COOH/H_2O_2$ experiments conducted as indicated above. Figure 2 shows *m*/*z* 32 (O_2^+) and 33 (HO_2^+) and the change in these peaks at three different temperatures: 412 °C, 455 °C, and 490 °C.

Peak 32 comes from essentially three sources: oxygen in the water, the electron ionization fragmentation of the hydrogen peroxide in the mass spectrometer ionizer, and the thermal decomposition of the peroxide. At low temperatures (T < 450 °C), the *m*/*z* 32 peak is absent to within the level of the

experimental uncertainty (noise) and indicates a negligible concentration of oxygen in the water and little ionization fragmentation of the peroxide to O_2^+. When temperatures in excess of 450 °C are reached, the oxygen peak appears and remains in the highest temperature experiment, but at a reduced signal strength indicating the depletion of the oxygen as the reaction proceeds.

The *m*/*z* 33 peak is expected to be due to the ionization fragmentation of the hydrogen peroxide at low temperatures and occurs as long as peroxide exists in the beam. When the peroxide is depleted, this peak should vanish and indicate when the peroxide has been completely decomposed. At the low-temperature experimental run, the *m*/*z* 33 peak is strong, but as the temperature increases to 455 °C, there is a steady decrease to zero in the *m*/*z* 33 peak. At the highest temperature, there is still no detectable *m*/*z* 33 peak to within experimental uncertainty. If HO_2^+ is generated during the initiation reaction (3 above) it should appear as a peak at *m*/*z* 33. This experiment shows no measurable HO_2^+ from the initiation reaction, during the high-temperature experiment. Later, using the mass peak detection mode experiments, we will show that both HO_2^+ and DO_2^+ can be measured in these experiments and could only be due to the initiation reaction.

Of note from Figure 2 is the mass resolution obtainable under these experimental conditions. This figure indicates that we can obtain up to at least 1 amu resolution under the given set of experimental conditions. From this result, we can expect that any measurable signal at a given mass is due primarily to the indicated mass and not signal spreading or tailing from mass peaks on either side. The fixed mass spectrometer settings used in all experiments result in a full width at half-maximum of less than 0.5 amu across the entire mass range probed.

II. Pyrolysis of Acetic Acid and Hydrogen Peroxide Decomposition. Pyrolysis experiments were conducted in the absence of any added oxidizer to investigate the thermal degradation of the acetic acid. We were looking for reactor operating conditions that would minimize any thermal degradation and allow us to measure the pure oxidation reaction. At these conditions, it would be possible to account for changes in the mass spectrometer detector output due to the oxidation reaction and we would not have to decouple any concurrent pyrolysis effects from the overall detector output signal. For mass spectrometer detection of acetic acid in solution, we monitored the *m*/*z* 45 peak (CO_2H^+), the strongest peak in the electron ionization fragment pattern for acetic acid. In the case of the fully deuterated acetic acid (CD_3COOD), we monitored the *m*/*z* 46 peak (CO_2D^+). The experiments with CH_3COOH were conducted with both H_2O and D_2O used as the solvent to determine if there is a measurable difference in the acetic acid fragment signal strength that could be attributed to solvent effects.

Figure 3 shows the CO_2H^+ signal versus temperature for both the H_2O and D_2O experiments. This figure shows that there is no measurable solvent effect on the CO_2H^+ signal. Figure 4 shows the CO_2D^+ signal versus temperature. Comparing Figures 3 and 4, there is no experimentally measurable difference for the H_2O/CH_3COOH, H_2O/CD_3COOD, and D_2O/CH_3COOH systems. All three curves indicate that to within experimental uncertainty, there is no measurable change in the acid concentration due to pyrolysis without an oxidizer. Pyrolysis of acetic acid under our experimental conditions is therefore not important and will have no affect on our oxidation experiments and corresponding analysis.

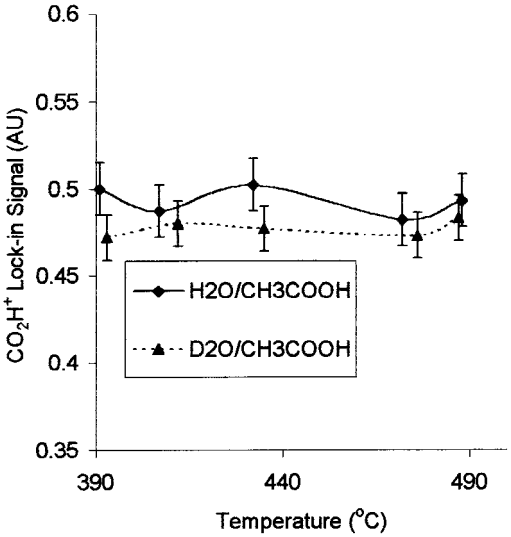

Figure 3. CO_2H^+ signal versus temperature in both H_2O and D_2O. Experimental systems: H_2O/CH_3COOH and D_2O/CH_3COOH.

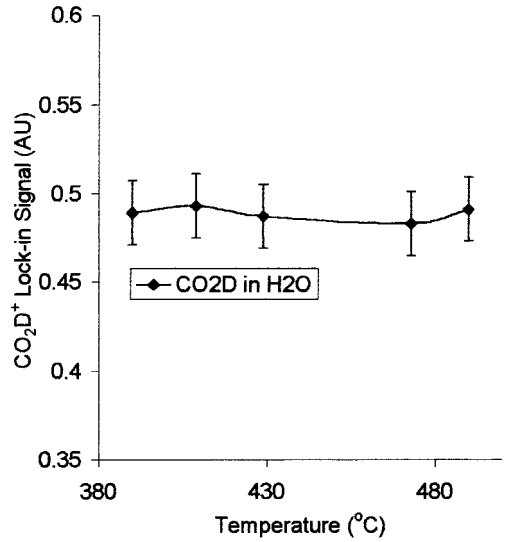

Figure 4. CO_2D^+ signal versus temperature in H_2O. Experimental system: H_2O/CD_3COOD.

Figure 5 shows the plot of the peroxide fragment HO_2^+ signal versus temperature in both H_2O and D_2O without acetic acid present. This figure confirms what was shown in Figure 2 above, the hydrogen peroxide is completely decomposed by 460 °C and without acetic acid present, this signal does not return. This result indicates that no measurable level of HO_2^+ is present in the system after all of the hydrogen peroxide decomposes. There is again no measurable change in signal, attributable to a solvent affect, when the water is changed from H_2O to D_2O.

III. Initiation Step and $HO_2^\bullet$ Radical Detection. Figures 6 and 7 show the results from the oxidation experiments for the $H_2O/CD_3COOD/H_2O_2$ system. Figure 6 shows the HO_2^+ and CO_2D^+ signals versus temperature while Figure 7 shows the DO_2^+ and DOH^+ signals versus temperature. The HO_2^+ signal, as above, indicates the relative concentration of hydrogen peroxide within the reactor while DO_2^+ is the mass signal corresponding to the $DO_2^\bullet$ radical generated during the initiation reaction step (3). With the $HO_2^\bullet$ radical generated during the reaction now shifted to $DO_2^\bullet$ by the use of deuterated acetic acid, it is seen that the small upward trend in the HO_2^+ signal observed in Figure 8 is absent, to within the experimental uncertainty for this experiment, and the signal for HO_2^+ looks

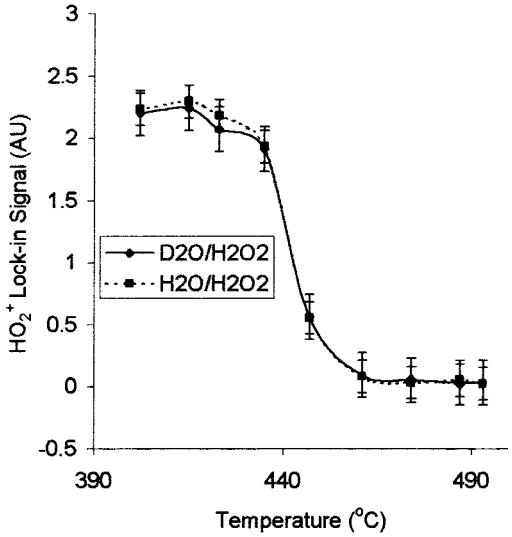

Figure 5. HO_2^+ signal versus temperature in H_2O and D_2O. Experimental systems: D_2O/H_2O_2 and H_2O/H_2O_2.

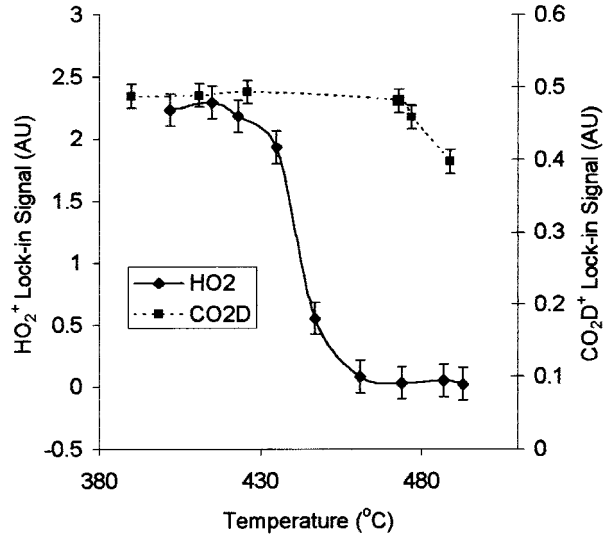

Figure 6. HO_2^+ and CO_2D^+ oxidation signals. Experimental system: $H_2O/CD_3CO_2D/H_2O_2$.

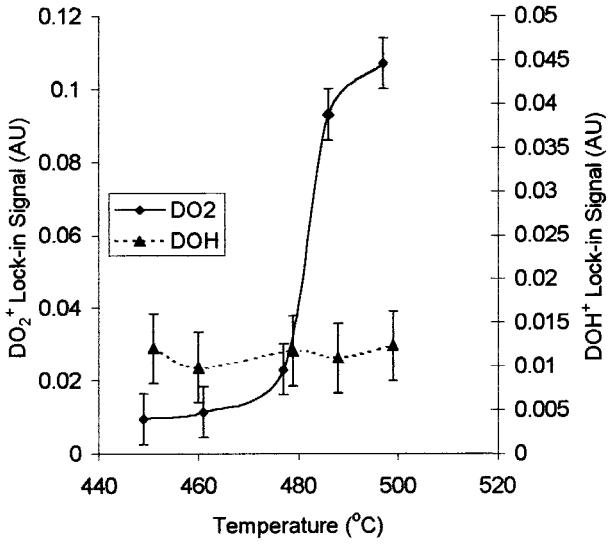

Figure 7. DO_2^+ and DOH^+ oxidation signals. Experimental system: $H_2O/CD_3COOD/H_2O_2$.

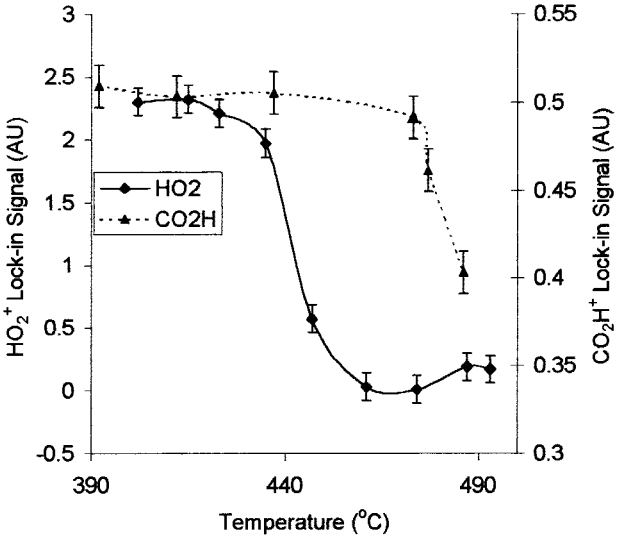

Figure 8. HO_2^+ and CO_2H^+ oxidation signals. Experimental system: $H_2O/CH_3COOH/H_2O_2$.

like the Figure 5 result for the peroxide fragment. The CO_2D^+ signal shows no detectable change below ~470 °C, then begins to decrease as the reaction proceeds. Figure 7 shows the corresponding DO_2^+ and DOH^+ signals from this same experiment. DO_2^+ is the isotopically shifted $HO_2^\bullet$ radical generated by the oxygen initiation step during the early stages of the oxidation reaction. The lack of any detectable DOH^+ signal indicates that the initiation step (4) involving the $HO^\bullet$ radical, generated by the hydrogen peroxide decomposition, is not an important initiation step during the early stages of the oxidation reaction probed in these experiments. The benchtop decomposition experiments conducted under the same experimental conditions as the DSMS experiments indicated that the decomposition of acetic acid is less than 5% for this microreactor design under the conditions of this study.

At low temperatures (T < 470 °C), the Figure 8 results below establish that the oxidation reaction does not proceed and the signal observed for the DOH^+ peak is simply noise. If the $HO^\bullet$ radical participated in the initiation step, the DOH^+ signal would increase as the temperature increases beyond the point where the reaction is known to initiate. Figure 7 indicates that this did not happen to within the experimental uncertainty of the lock-in amplifier output at this mass. The DO_2^+ signal shown in Figure 7 indicates that this radical is generated by the oxygen initiation step (3). This result confirms the assessment that will be given in the analysis of Figure 8 below, the upward trend in the HO_2^+ signal at the higher temperatures is due to the generation of the $HO_2^\bullet$ radical by the oxygen initiation step (3).

An experimental oxidation experiment for the $H_2O/CH_3COOH/H_2O_2$ system is shown in Figure 8. The plot shows the HO_2^+ and CO_2H^+ signals versus temperature. The CO_2H^+ signal shows no measurable change below ~470 °C, in accordance with the results above. The hydrogen peroxide concentration decreases to zero at ~450 °C, as indicated by the fragment HO_2^+ signal, and this result suggests that there is no direct oxidation of the acetic acid by the hydrogen peroxide. This result validates the reaction mechanism's initiation steps, which only include oxygen and the $HO^\bullet$ radical, both generated by the decomposition of hydrogen peroxide, as possible initiators for the oxidation reaction.

Above ~480 °C, the HO_2^+ signal shows an increase just greater than the experimental uncertainty. When comparing this result with the result from Figure 5, where no upward trend in the HO_2^+ signal is measured, outside of experimental uncer-

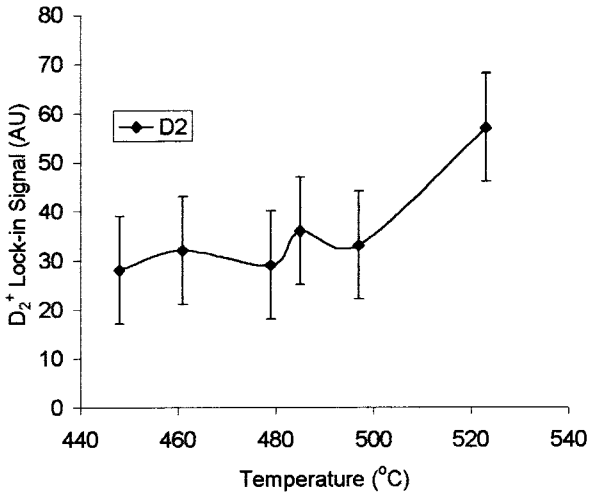

Figure 9. D_2^+ signal versus temperature (water incorporation). Experimental system: $D_2O/CH_3COOH/H_2O_2$.

tainty, for the temperature range exceeding 480 °C, the signal increase shown by Figure 8 can be argued to be the generation of $HO_2^\bullet$ from the oxidation reaction's initiation step (3), as shown in the above reaction mechanism. This same experiment is run for the $D_2O/CH_3COOH/H_2O_2$ system with the result that no experimentally significant difference existed between the two. This result again indicates that the supercritical water has no measurable effect on the reaction mechanism or the observable kinetics. Any participation by the supercritical water in the bond breaking or bond forming reactions of the overall oxidation reaction would be observed by a deuterium kinetic isotope effect, where it would be expected that a decrease in the overall reaction kinetics would be measured by a change in the signal versus temperature plots.

IV. Water Incorporation. The final experiment conducted was to investigate the extent of participation by the supercritical water in the reaction mechanism. As stated above, for this part of the experiment the reduced mechanistic model was modified to include the water gas shift reaction, step 9:

$$CO + H_2O \rightarrow HCOOH \rightarrow CO_2 + H_2$$

With the $D_2O/CH_3COOH/H_2O_2$ system, there are two available sources of water, the supercritical D_2O bath and the H_2O generated during the reaction. This results in either the generation of H_2 or D_2 depending on which water source is participating in the water gas shift reaction. Figure 9 is the plot of the D_2^+ signal versus temperature resulting from the $D_2O/CH_3COOH/H_2O_2$ oxidation experimental system. There are two sources for the D_2^+ signal in this experiment. The first source is D_2^+ coming from the fragmentation of D_2O in the mass spectrometer ionizer and the second source is the D_2 generated by the water gas shift reaction. At low temperatures, below 470 °C, there is no measurable oxidation reaction and the D_2^+ signal is simply the baseline value for D_2O water bath fragmentation. As temperature is increased above the point where the oxidation reaction is known to initiate, any generation of D_2 should be measured by an increase in the D_2^+ signal level above this baseline value. Figure 9 shows that there is no measurable increase in the D_2^+ signal up to 500 °C. This would indicate that the water gas shift reaction is not important in the overall reaction scheme up to 500 °C and that the D_2O solvent water is acting strictly as a thermal bath and is not participating in the overall reaction.

A final experiment was conducted where the microreactor temperature was increased to 523 °C and the $D_2O/CH_3COOH/H_2O_2$ system was again run. This was primarily done to extend the reactor conditions and the DSMS system to experimental limits that had not been reached in earlier experiments. During the course of this experiment, the D_2^+ signal was seen to markedly increase from the low-temperature baseline value, indicating the possible generation of D_2 from the water gas shift reaction involving the D_2O bath water. This high temperature experimental run was conducted only once, but was reproduced by all three identical sample runs that constitute a single experiment. The best assessment we can give of this result at this time is that up to 500 °C there is no measurable participation by the bulk water molecules in the overall oxidation reaction. This is in accordance with the results shown above in Figures 6−8, where it was shown that the change from H_2O to D_2O in the oxidation experiments did not result in any measurable change in the CO_2H^+ signal versus temperature. The limited data involving the detection of a D_2^+ signal, above the low-temperature baseline value, at a temperature of 523 °C indicated that the bulk water might participate in the overall supercritical water oxidation reaction. Boock et al.[32] was able to show that supercritical water does participate in hydrolysis reactions and to some extent in pyrolysis reactions. Melius et al.[33] modeled reaction thermochemistry in supercritical water and showed that their results were consistent with the participation of the water in bond breaking and bond forming reactions. These results were obtained for temperatures exceeding 500 °C and would seem to be consistent with the result from our single experimental run above 500 °C. This consistency would then also suggest that the absence of a detectable change below 500 °C in our experiments is also real, indicating that the water does not participate in the reaction chain mechanism at these lower temperatures.

Conclusion

We have successfully coupled a quartz capillary microreactor operating in the supercritical fluid region of water at temperatures and pressures of 400−500 °C and 23−28 MPa, respectively, with a direct sampling mass spectrometry system. With this system, we are able to directly observe several of the reaction intermediates and free-radicals included in most elementary reaction schemes for the supercritical water oxidation of acetic acid. In this experimental design, we found that critical parameters for the coupling of the high-pressure and temperature supercritical water microreactor with the DSMS system are the sensitive positioning of the nozzle in relation to the skimmer and the sharpness of the skimmer tip.

This DSMS system allowed us to directly study the oxidation mechanism of acetic acid in supercritical water. We were able to investigate a few important questions relevant to the supercritical water oxidation of organic species. We have successfully measured, for the first time, the $HO_2^\bullet$ free radical species thought to be important in the overall oxidation mechanism. Also, we studied the initiation step of the oxidation reaction and showed that it proceeds by hydrogen abstraction from the acetic acid primarily by the O_2 species and not the $HO^\bullet$ radical, at least in the early stages of the reaction, where greater than 95% of the initial acetic acid remains. Finally, we investigated the extent of incorporation of the bulk supercritical water into the oxidation mechanism and we were able to show that below 500 °C, there is no incorporation of the supercritical water into the reaction mechanism. The supercritical water simply serves to maintain a well-mixed, single-phase reaction environment.

We have shown that the DSMS technique has the potential to be a valuable tool. Further work is required to demonstrate

that this approach can provide the necessary details of the reaction mechanisms taking place in the SCWO of organic waste streams that would provide for more accurate engineering scale-up design from the experimental bench-scale to the operational full-scale reactor facility.

Acknowledgment. We thank Dr. Morton Fineman for his work with the electropolishing technique used to sharpen the skimmer tip. Thanks are also due to Ms. Lindsey Govreau for her help with the TOF data collection and the testing of the quartz capillary nozzle manufacturing process.

References and Notes

(1) Modell, M. *Standard Handbook of Hazardous Waste Treatment and Disposal*; McGraw-Hill: New York, 1989.
(2) Tester, J. W.; Holgate, H. R.; Armellini, F. J.; Webley, P. A.; Killilea, W. R.; Hong, G. T.; Barner, H. E. *ACS Symposium Series 518: Emerging Technologies in Hazardous Waste Management III*; Am. Chem. Soc., Washington, DC, 1993.
(3) *Haz. Waste Consult.* **Jan.-Feb. 1999**, *17* (1), A1.11.
(4) Schmieder, H.; Abeln, J. *Chem. Eng. Technol.* **Nov. 1999**, *22* (11), 903.
(5) Aki, S. N. V. K.; Abraham, A. *Environ. Prog.* **Winter 1998**, *17* (4), 246.
(6) Cansell, F.; Beslin, P.; Berdeu, B. *Environ. Prog.* **Winter 1998**, *17* (4), 240.
(7) Rice, S. F.; Steeper, R. R. *J. Haz. Mater.* **Apr. 1998**, *59* (2−3), 261.
(8) Holgate, H. R.; Tester, J. W. *Combust. Sci. Tech.* **1993**, *88*, 369.
(9) Brown, M. S.; Steeper, R. R. *Appl. Spectrosc.* **1991**, *45*, 1733.
(10) Myrick, M. L.; Kolis, J.; Parsons, E.; Chike, K.; Lovelace, M.; Scrivens, W.; Holiday, R.; Williams, M. *J. Raman Spec*trosc. **1994**, *25*, 59.
(11) Rice, S. F.; Hunter, T. B.; Ryden, A. C.; Hanush, R. G. *Ind. Eng. Chem. Res.* **1996**, 35, 2161.
(12) Barner, H. E.; Huang, C. Y.; Johnston, T.; Jacobs, G.; Martch, M. A.; Killilea, W. R. *J. Hazard. Mater.* **1992**, *31*, 1.
(13) Bramlette, T. T.; Mills, B. E.; Hencken, K. R.; Brynildson, M. E.; Johnston, S. C.; Hruby, J. M.; Feemster, H. C.; Odegard, B. C.; Modell, M. *Sandia Nat. Lab. Rep.*, SAND90-8229, 1990.
(14) Ikushima, Y.; Arai, M. *Chem. Phys.* **1998**, *238*, 455−464.
(15) Chlistunoff, J. B.; Johnston, K. P. *J. Phys. Chem. B* **1998**, *102*, 3993−4003.
(16) Groeger, W.; Fenn, J. B. *Rev. Sci. Instrum.* **1988**, *59*, 1971.
(17) Randall, L. G.; Wahrhaftig, A. L. *Anal. Chem.* **1978**, *50*, 1703.
(18) Randall, L. G.; Wahrhaftig, A. L. *Rev. Sci. Instrum.* **1981**, *52*, 1283.
(19) Fukuoka, H.; Imasaka, T.; Ishibashi, N. *Anal. Chem.* **1986**, *58*, 375.
(20) Syage, J. A. *Anal. Chem.* **1990**, *62*, 505A.
(21) Smith, R. D.; Fulton, J. L.; Petersen, R. C.; Kopriva, A. J.; Wright, B. W. *Anal. Chem.* **1986**, *58*, 2057.
(22) Lustig, D. A.; Lubman, D. M. *Rev. Sci. Instrum.* **1991**, *62*, 957.
(23) Maharrey, S. P. Ph.D. Dissertation. Department of Applied Mechanics and Engineering Sciences, University of California, San Diego, UMI Ref. #9906496, 1998.
(24) Maharrey, S. P.; Miller, D. R. *AIChE J.*, to be published.
(25) Lee, D. S.; Gloyna, E. F.; Li, L. *J. Supercrit. Fluids* **1990**, *3*, 249.
(26) Wightman, T. J. MS Thesis. University of California, Berkeley, 1981.
(27) Rice, S. F.; Steeper, R. R.; LaJeunesse, C. A. *Sandia Nat. Lab. Rep.*, SAND94-8203, 1993.
(28) Miller, D. R. *Atomic and Molecular Beam Methods*; Oxford: New York, 1988; Vol. 1, Chapter 2.
(29) Boock, L. T.; Klein, M. T. *Ind. Eng. Chem. Res.* **1993**, *32*, 2464.
(30) Boock, L. T.; Klein, M. T. *Ind. Eng. Chem. Res.* **1994**, *33*, 2554.
(31) Lin, C. C.; Smith, F. R.; Ichikawa, N.; Baba, T.; Itow, M. *Int. J. Chem. Kinet.* **1991**, *23*, 971.
(32) Boock, L.; Wu, B.; LaMarca, C.; Klein, M.; Paspek, S. *Chemtech.* **Dec. 1992**, *23*, 719.
(33) Melius, C. F.; Bergan, N. E.; Sheperd, J. E. *23rd Symposium (International) on Combustion*; The Combustion Institute: Pittsburgh, PA, 1991.